Mem. S.A.It. Suppl. Vol. 19, 284

Memorie della
Supplementi

The UV Luminosity Function of $z \sim 7$ galaxies from wide and deep HST and ESO/VLT surveys

A. Grazian[1], L. Pentericci[1], M. Castellano[1], and A. Fontana[1]

Istituto Nazionale di Astrofisica – Osservatorio Astronomico di Roma, Via Frascati 33, I-00040 MontePorzio Catone (Roma), Italy e-mail: grazian@oa-roma.inaf.it

Abstract. The study of the Luminosity Function (LF) of Lyman Break Galaxies (LBGs) at z=7 is very important for ascertaining their role in the reionization of the Universe. In this work we plan to perform a robust determination of the UV LF for LBGs at $z \sim 7$. To this aim, we have assembled a large sample of candidate LBGs at $z \sim 7$ from different surveys, spanning a large variety of areas and depths. In particular, we have combined data from the deep ($J < 27.4$) and ultradeep ($J < 29.2$) surveys recently acquired with the new WFC3 NIR camera on HST, over the GOODS-ERS (~40 sq. arcmin.) and the HUDF (~4 sq. arcmin.) fields, with a ground based survey in wide and relatively shallow areas (~200 sq. arcmin.) from Hawk-I@VLT. We have used public images in the z band to select z-dropout galaxies, and other public data both in the blue (UBVRI) and in the red bands to reject possible low-redshift interlopers. We have found that the number density of faint LBGs at $z \sim 7$ is strongly dependent on the assumption made on the half light distributions of the simulated galaxies, used to correct the observed sample for incompleteness. We conclude that galaxies at $z \sim 7$ are unable to reionize the Universe unless there is a significant evolution in the clumpiness of the inter-galactic medium (IGM) or in the escape fraction of ionising photons or, alternatively, there is a large population of $z \sim 7$ LBGs with large physical dimensions but still not detected by the present observations.

Key words. Galaxies:distances and redshift – Galaxies: evolution – Galaxies: high redshift – Galaxies: luminosity function.

1. Introduction

The detailed understanding of the physical properties of the first building blocks of present-day galaxies is fundamental to set the zero point for the theoretical models dealing with the formation and evolution of galactic structures in the Universe. In particular, the study of the faint end of the UV LF of z=7 LBGs is very important for understanding their contribution to the reionization processes of the high-z Universe.

At $z \sim 6$ the Universe is almost re-ionized (Fan et al. 2006; Becker et al. 2007) and there is both observational (Meiksin 2009; Komatsu et al. 2010) and theoretical (Gnedin & Fan 2006; Cen 2010) mounting evidence that the crucial transformation from neutral to ionized state should happen around $z \sim 9$. The exact timescale of the reionization process, however, is not clear, the alternatives going from an ex-

Send offprint requests to: A. Grazian

tended period, $z \sim 7-11$ (Dunkley et al. 2009), to a more sudden transition (Cen 2003).

The new SUBARU (Ouchi et al. 2009), Hawk-I (Castellano et al. 2010a,b, hereafter C10a and C10b), and WFC3 (Bouwens et al. 2010) surveys have started investigating the properties of galaxies during the reionization epoch, enlarging the small sample of galaxy candidates at $z \sim 7$ sketched by NICMOS (Bouwens & Illingworth 2006; Oesch et al. 2007). Recently, Oesch et al. (2010) derived the number density of faint LBGs at z=7 in the HUDF, concluding that these low luminosity galaxies are enough to reionize the Universe, assuming that the IMF, the clumpiness of the IGM, the escape fraction of ionising photons and their metallicity have not significantly evolved with respect to their local properties. Using the same data-set, McLure et al. (2010) found that it would be difficult for the observed population of high-redshift star-forming galaxies to achieve reionization by $z \sim 6$ without a significant contribution from galaxies well below the detection limits, together with significant variations in the escape fraction of ionising photons.

The different results obtained for the LF of LBGs at z=7 should be ascribed both to the different data-sets used and to the different techniques adopted to analyse the data. We want to study in detail the possible systematics/uncertainties in the LF estimate, in particular due to the statistical tools used in the LF derivation. Moreover, extending the LF at z=7 down to faint magnitude limits is fundamental to break current degeneracies between M^* and Φ^*, and to put strong constraints on the number density of faint LBGs at high-z. Here we combine a re-analysis of the extremely deep WFC3 observations (Oesch et al. 2010) with the selection of bona-fide $z \sim 7$ LBGs in wide areas of the sky (C10a, C10b, Ouchi et al. 2009) in order to derive stringent constraint to the reionization process at $z \sim 7$.

Throughout the whole paper, observed and rest–frame magnitudes are in the AB system, and we adopt the Λ-CDM concordance model ($H_0 = 70 km/s/Mpc$, $\Omega_M = 0.3$ and $\Omega_\Lambda = 0.7$).

2. The Data

We have analysed two different data-sets observed with the new NIR camera of HST, the Wide Field Camera 3 (WFC3): the Early Release Science on the GOODS-S field (GOODS-ERS) and the Hubble Ultra Deep Field (HUDF) programs. We have complemented this dataset with the wide area covered by the Hawk-I imager in the Y band, described in detail in C10a and C10b.

2.1. ERS

The GOODS-ERS WFC3/IR dataset is a total of 60 HST orbits consisting of 10 contiguous pointings in the GOODS-South field (HST Program ID 11359), using 3 filters per visit (Y_{098}, J_{125}, H_{160}), and 2 orbits per filter (for a total of 4800-5400s per pointing and filter). The total area covered by the GOODS-ERS is $\sim$ 40 sq. arcmin. till Y=27.3, J=27.4, and H=27.4 magnitudes at 5σ in an area of ~ 0.11 sq. arcsec (corresponding to 2 times the FWHM of the images).

The WFC3 ERS images were reduced using the Multidrizzle software (Koekemoer et al. 2002), adopting on-orbit SPARS100 darks and also correcting for the gain differences between different quadrants. Large-scale residuals on each exposure which are apparently due to scattered light have been removed, and the satellite trails have been masked on affected exposures. The astrometry of the images is bound to the GOODS-S v2.0 z-band (Giavalisco et al. 2004). The matching is robust even for a single exposure, with 400-600 sources matching, so that the overall alignment seems to be robust to a level of $\sim 10 mas$. The pixel size of the reduced images is 0.06 arcsec, with a PSF of 0.18 arcsec.

2.2. HUDF

The HUDF WFC3/IR dataset (HST Program ID 11563) is a total of 60 HST orbits in a single pointing (Oesch et al. 2010; Bouwens et al. 2010) in three broad-band filters (16 orbits in Y_{105}, 16 in J_{125}, and 28 in H_{160}). It is the deepest NIR image ever taken, reaching Y=29.3, J=29.2, and H=29.2 magnitudes at 5 sigma in $\sim$ 0.11 sq. arcsec. The area covered by the WFC3-HUDF imaging is 4.7 sq. arcmin., and the IR data have been drizzled to the ACS-HUDF data (Beckwith et al. 2006), with a resulting pixel scale of 0.03 arcsec, with a PSF of 0.18 arcsec. The HUDF images were reduced in the same way as the ERS dataset.

2.3. Hawk-I

The ESO wide field NIR imager, Hawk-I, recently installed at the VLT, is an ideal instrument to search for bright and rare galaxies at very high redshift.

More than 100 hours of Hawk-I were allocated during Science Verification and from a Large Program (PI A. Fontana) to observe four Hawk-I fields down to a magnitude limit of $Y = 26.7$ for a total area of ~200 sq. arcmin. The images have been reduced with standard techniques for NIR images, and the coadded frames have a FWHM of 0.5 arcsec. A detailed description of this survey can be found in C10a and C10b.

2.4. Comparison between Hawk-I and WFC3

Thanks to its wide field of view (7.5 by 7.5 sq. arcmin.) and its high throughput, the Hawk-I imager is a competitor to WFC3 when large areas should be covered at relatively shallow flux limits ($Y \sim 26.5$), as shown in Fig.1. On the top-left, a zoom of 15 hours of Hawk-I data in the Y band is compared to 1.5 hours of WFC3 (top-right) on the same pointing in the ERS field. The area covered by Hawk-I, however, is 10 times larger, resulting in a similar survey efficiency of WFC3. Of course, when very deep imaging is required, WFC3 is unrivalled, as shown in the bottom part of Fig.1.

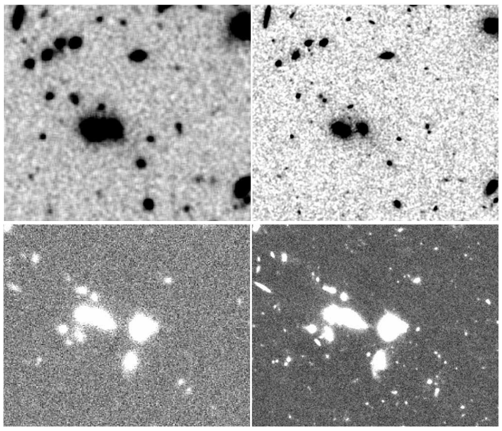

Fig. 1. *Top panels*: The Hawk-I image (left) is compared with the WFC3 pointing (right) for the same positions on the ERS field. *Bottom panels*: the same comparison for the HUDF field.

3. Candidate selection and Simulations

The selection of galaxies at $z \sim 7$ uses the well known "drop-out" or "Lyman-break" technique. At $6.5 < z < 7.5$, this feature is sampled by the large $Z - Y$ color, as shown in Figure 2 for the HUDF field.

We propose a modification of the Oesch et al. (2010) criterion, based on simple considerations. We adopt the same color criteria:

$$z - Y_{105} > 0.8,$$
$$z - Y_{105} > 0.9 + 0.75(Y_{105} - J_{125}),$$
$$z - Y_{105} > -1.1 + 4.0(Y_{105} - J_{125})$$

for the HUDF and

$$z - Y_{098} > 1.1,$$
$$z - Y_{098} > 0.55 + 1.25(Y_{098} - J_{125}),$$
$$z - Y_{098} > -0.5 + 2.0(Y_{098} - J_{125})$$

for the ERS.

For the non-detection in bands bluer than Z, we adopt the same criteria used in C10a and C10b ($S/N < 2$ in all BVI bands and $S/N < 1$ in at least two of them). We apply however only a single cut in the J magnitude ($J < 29.2$ for the HUDF and $J < 27.4$ for the ERS), since this band corresponds to 1500Å rest frame. We avoid the double selection $S/N(J) > 5$ and $S/N(Y) > 5$, as adopted by Oesch et al. (2010), since it could be less sensitive to red galaxies in the $Y - J$ color at faint J magnitudes.

Fig.2 shows the Z-Y vs Y-J color plot for the HUDF field.

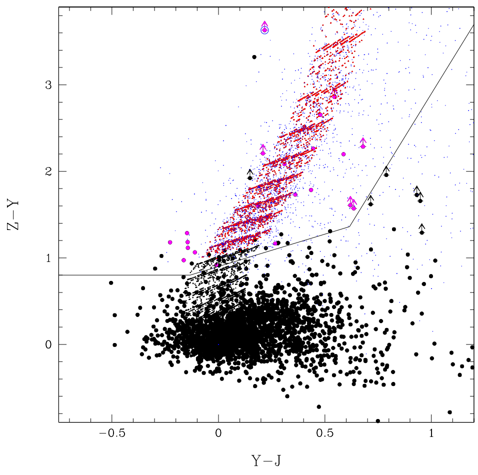

Fig. 2. The $Z - Y$ vs $Y - J$ color-color diagram for the HUDF dataset limited at $J < 29.2$. Big points are observed galaxies, small black points are CB07 models at $0.0 < E(B - V) < 0.3$, with small red points those at $z > 6.5$. The small blue points are the result of our simulations, with synthetic objects inserted in the FITS images and recovered using the same procedure used for the observed catalog. The solid line shows our color criterion. Candidate galaxies at $z \sim 7$ are shown in magenta. Vertical arrows are upper limits in the Z band, while the blue circle at $Z - Y > 3.6$ is the suspected SNa outlined by Oesch et al. (2010).

For the Hawk-I fields the color criteria adopted is similar to the one for WFC3, namely $Z - Y \geq 1$, with the exception that the limiting magnitude in the J or K band is much shallower than the one in the Y band. For this reason, only very red and dead galaxies or cold L-T dwarf stars with $Y - J \geq 1.5$ or $Y - K \geq 2.0$ were excluded. For the non-detection in bands bluer than Z, we adopt the same criteria described above ($S/N < 2$ in all BVI bands and $S/N < 1$ in at least two of them).

Following the $z \sim 7$ criteria, we select 20 candidates in the HUDF field, in the ERS we find 22 z-dropout candidates, while in the four Hawk-I fields we have found a total of 22 bona fide $z \sim 7$ galaxies. We have excluded from these candidates the bright transient (probably a SNa), outlined by Oesch et al. (2010) in the HUDF field (blue circle in Fig.2 at $Z - Y > 3.6$).

3.1. Simulations

While the selection criteria described above are formally designed to select a pure sample of high-z candidates, they are in practice applied to very faint objects, typically close to the limiting depth of the images. At these limits, systematics may significantly affect their detection and the accurate estimate of their large color terms. To take into account all the systematic effects (completeness, photometric scatter) involved in the LF estimate, we carried out a set of detailed simulations, with the aim of deriving the LF. We first produce a set of (M_{1500}, z) according to a given distribution, convert them into observed magnitudes, insert into the real images the synthetic sources and then extract them using the same recipes adopted for the observed catalog. This process gives both the completeness corrections and the transfer function, needed to derive the best fit for the UV LF at $z \sim 7$. The typical half light radius of the simulated galaxies spans from 0.1 arcsec (compact morphologies) to 0.25 arcsec (extended morphologies). Details can be found in C10a, C10b, and Grazian et al. (2010).

4. Results

The steepness of the faint end of the LF, α, depends critically on the half light radii of the synthetic galaxies used to carry out the simulations. In Fig.3 we show the half light radii of the different morphological templates against the best fit α of the LF. For large value of the half light radius, namely > 0.2 arcsec, the best fit α is between -1.8 and -1.9, as found by Oesch et al. (2010) and Bouwens et al. (2010) at z=7 and beyond. For smaller values, ~ 0.1 arcsec, we find α in the range -1.4 to -1.7, in agreement with McLure et al. (2010) that have used point sources as input for their simulations. The uncertainties on this parameter, α, are still large, of the order of $\sim 0.2 - 0.4$. *We find a significant relation between the half light radius and α, indicating that simple conclusions based on the LF at $z \sim 7$ depends dramatically on the half light radius distribution assumed for the simulations.*

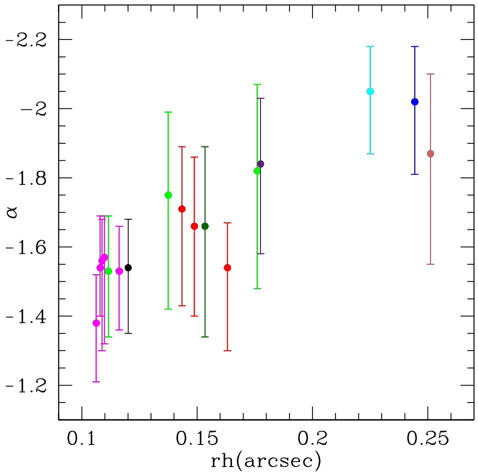

Fig. 3. The dependence of the steepness of the LF, α, against the half light radii of the simulated galaxies. Different colors indicate the various adopted morphologies.

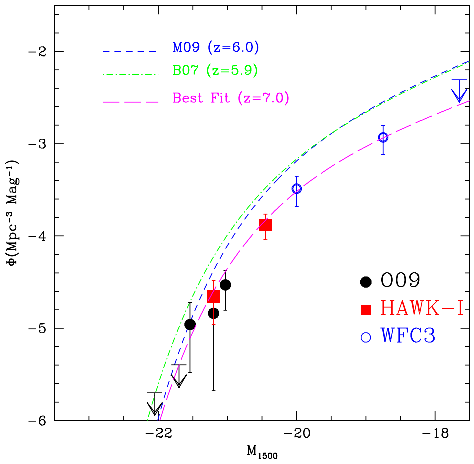

Fig. 4. The resulting LF of LBGs at $z \sim 7$. The LF at z=7, obtained using as morphological templates the stack of the faint candidates ($J \geq 27.5$) selected in the HUDF, has been derived using WFC3 data (ERS+HUDF) for the faintest bins (blue circles). The red squares represent the LF found in the Hawk-I from C10a and C10b, while the black circles and arrows indicates the measurement of Ouchi et al. (2009). The magenta line is the best fit to the points at $z \sim 7$. The blue dashed and green dot-dashed lines show the LF at z=6 of McLure et al. (2009) and Bouwens et al. (2007), respectively.

Here we adopt as a reference case only the stack of the faint candidates ($J \geq 27.5$) selected in the HUDF (black dot in Fig.3), and then derive the LF for the WFC3 data (ERS+HUDF), as shown in Fig.4. We add to these data from space the results of the two ground based surveys by Hawk-I (C10a and C10b) and by SUBARU (Ouchi et al. 2009).

All the observed points shown in Fig.4 have been used to fit the LF. We scan the parameter space in 3D (Φ^*, M^*, and α) adopting a Schechter parameterization (Schechter 1976) and taking into account the asymmetric errors and the presence of upper limits. The best fit is shown and it is compared to the LFs at z=6 of Bouwens et al. (2007) and McLure et al. (2009). Using our best fit, we provide a robust estimate of the LF at $z = 7$, excluding at >99.73% c.l. ($> 3\sigma$) the non-evolution from z=6 to z=7. Indeed, we are able to show that the normalization at $M_{1500} \sim -19$ is significantly lower than the LF at $z \sim 6$. Moreover, combining data with a large range in absolute magnitudes we are able to reduce the degeneracies in the three parameters of the LF.

5. Discussion

We discuss the implications on reionization derived from our best fit LF and the uncertainties on the LF parameters implied by the assumption made during completeness simulations. The rate of ionizing photons needed to balance the recombination process of hydrogen in the IGM and hence to keep the Universe reionized is $\dot{N}_{ion} \geq 10^{47.4} C_{HII}(1+z)^3$, that translates into a constraint to the clumpiness of the IGM to be $C_{HII} \leq (\rho_{UV} f_{esc})/(3 \cdot 10^{22} \alpha_S (1+z)^3)$. The relevant UV emissivity of LBGs ρ_{UV} is computed by integrating the LF down to $M_{1500} = -10$ (Bouwens et al. 2010), assuming that the steepness of the faint end of the LF remains constant; we have no information on the number density of $z \sim 7$ galaxies at these faint magnitudes with the present data.

The reionization rate $\dot{N}_{ion}$ however depends largely on the contribution of faint galaxies ($-19 \leq M_{1500} \leq -10$), since $\rho_{UV}(M_{1500} < -10)$ could be 10-15 times larger than $\rho_{UV}(M_{1500} < -19)$ if the LF is steeper than $\alpha \leq -2$. This is eventually still possible, if a large number of faint and extended galaxies exist. If the faint end of the LF at z=7 is not so steep, as we have inferred here for the compact morphologies, the contribution of fainter galaxies ($-19 \leq M_{1500} \leq -10$) is only 2.4 times that of $M_{1500} \leq -19$ LBGs. *Thus, the present uncertainty on the steepness of the faint end of the LF translates in a large uncertainty, of a factor 2-15, on the best fit of the luminosity density, SFR density, and reionization rate at z=7.*

Following Windhorst et al. (2002), it is plausible that fainter galaxies have smaller physical sizes: in this case a combination of high escape fraction ($f_{esc} \geq 0.2$) and small clumpiness ($C_{HII} \leq 3$) is required for the reionization of the Universe (see Grazian et al. (2010) for more details). It is worth noticing that the recent estimates of f_{esc} for $L \geq L^*$ LBGs at $0 \leq z \leq 3$ are ≤ 0.15 (Bridge et al. 2010; Cowie et al. 2010; Siana et al. 2010; Vanzella et al. 2010), implying a consistent evolution of the galaxy escape fraction going to fainter luminosities or to higher redshifts.

Acknowledgements. Based on observations made with the NASA/ESA Hubble Space Telescope, obtained from the data archive at the Space Telescope Institute. STScI is operated by the association of Universities for Research in Astronomy, Inc. under the NASA contract NAS 5-26555. Observations were also carried out using the Very Large Telescope at the ESO Paranal Observatory under Programme IDs LP181.A-0717, LP168.A-0485, ID 170.A-0788, ID 181.A-0485, ID 283.A-5052. We acknowledge partial financial support from ASI.

References

Becker, G. D., Rauch, M., Sargent, W. L. W. 2007, ApJ, 662, 72
Beckwith, S. V. W., Stiavelli, M., Koekemoer, A. M., et al. 2006, AJ, 132, 1729
Bouwens, R. J. & Illingworth, G. D., 2006 Nature, 443, 189
Bouwens, R. J., Illingworth, G. D., Franx, M., & Ford, H. 2007, ApJ, 670, 928
Bouwens, R. J., Illingworth, G. D., Oesch, P. A., et al. 2010, arXiv:1006.4360
Bridge, C. R., Teplitz, H. I., Siana, B., et al. 2010, ApJ, 720, 465
Castellano, M., Fontana, A., Boutsia, K., et al. 2010a, A&A, 511, 20; C10a
Castellano, M., Fontana, A., Paris, D., et al. 2010b, A&A, 524, 28; C10b
Cen, R., 2003, ApJ, 591, 12
Cen, R., 2010 ApJL submitted, arXiv:1007.0704
Cowie, L. L., Barger, A. J., & Hu, E. M. 2010, ApJ, 711, 928
Dunkley, J., Komatsu, E., Nolta, M. R., et al. 2009, ApJS, 180, 306
Fan, X., Strauss, M. A., Becker, R. H., et al. 2006, AJ, 132, 117
Giavalisco, M., Dickinson, M., Ferguson, H. C., et al. 2004, ApJ, 600, L103
Gnedin, N. Y. & Fan, X. 2006, ApJ, 648, 1
Grazian, A., Castellano, M., Koekemoer, A. M., et al. 2010, A&A submitted, arXiv:1011.6569
Koekemoer, A. M., Fruchter, A. S., Hook, R., Hack, W., 2002, HST Calibration Worskhop (eds. S. Arribas, A. Koekemoer, B. Whitmore, STScI: Baltimore), 337
Komatsu, E., Smith, K. M., Dunkley, J., et al. 2010, arXiv:1001.4538
McLure, R. J., Cirasuolo, M., Dunlop, J. S., et al. 2009, MNRAS, 395, 2196
McLure, R. J., Dunlop, J. S., Cirasuolo, M., et al. 2010, MNRAS, 403, 960
Meiksin, A. A., 2009, RvMP, 81, 1405
Oesch, P. A., Stiavelli, M., Carollo, C. M., et al. 2007, ApJ, 671, 1212
Oesch, P. A., Bouwens, R. J., Illingworth, G. D., et al. 2010, ApJ, 709L, 16
Ouchi, M., Mobasher, B., Shimasaku, K., et al. 2009, ApJ, 706, 1136
Schechter, P. 1976, ApJ, 203, 297
Siana, B., Teplitz, H. I., Ferguson, H. C., et al. 2010, arXiv:1001.3412
Vanzella, E., Giavalisco, M., Inoue, A., et al. 2010, arXiv:1009.1140
Windhorst, R. A., Cohen, S., Jansen, R., et al. 2002, AAS, 201, 3207